Supporting Information for:

"Polymer-Based Mesh as Supports for Multi-layered 3D Cell Culture and Assays"

Karen A. Simon, Kyeng Min Park[§], Bobak Mosadegh[§], Anand Bala Subramaniam[§], Aaron D. Mazzeo, Phil M. Ngo and George M. Whitesides*

Department of Chemistry & Chemical Biology and
Wyss Institute for Biologically Inspired Engineering
Harvard University, Cambridge, MA 02138

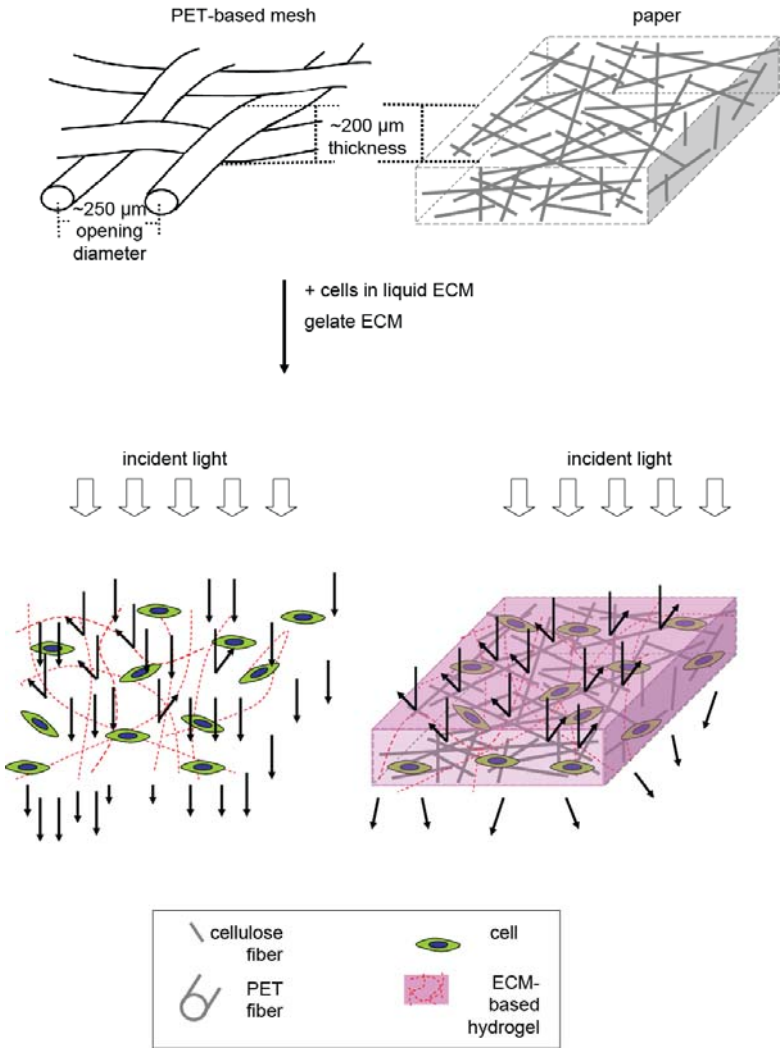

Figure S-1. Schematic showing the cross-section of PET-based mesh and paper-based supports and the path light travels through CiGiM and CiGiP.

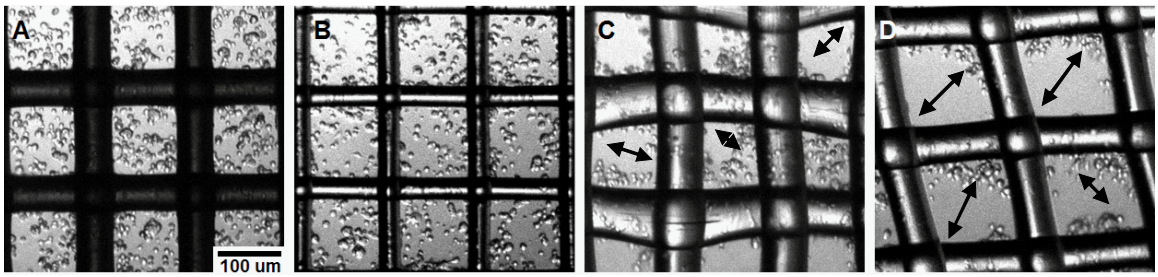

Figure S-2. MDA-MB231 cells cultured on meshes made from different materials. A suspension of cells in Matrigel (1×10^7 cells/mL) was seeded on meshes of (A) Polyester (B) PEEK (C) Polypropylene (D) Nylon. Optical images were taken with a light microscope after 24 h of culture. Arrows indicate regions of the mesh where gels have fallen off.

Measurement of Contact Angles on Polymer-based Mesh Supports

We measured the apparent contact angle of water on the mesh using an Advanced Goniometer System (Ramé-Hart, Inc.) to obtain an indication of the changes in the surface characteristics of the polymeric mesh material due to surface treatment. We suspended the mesh by using two 1-mm thick microscope glass slides as spacers to prevent the mesh from touching the surface of the sample stage. A drop of water (~10 uL) was dispensed carefully onto the mesh sheets with a micropipette. The droplet rested on both the polymeric material of the mesh and on air in the voids of the mesh, thus forming a composite contact zone. In this configuration, the edge of the droplets was pinned on the polymeric threads of the mesh forming stable sessile drops. For each mesh sample, we obtained contact angles from three identical drops of water; and measured contact angled from the left and right sides of each drop. The reported contact angles in Table S-1 represent an average of eight measurements for each type of mesh sample.

Table S-1 Contact Angles of the mesh before and after treatment

treatment method	exposure/incubation time	contact angle (Θ), °	% decrease in Θ[a]
no treatment	N/A	113 ± 3	N/A
air plasma	30 min each side (60 min/sheet)	23 ± 3	79 ± 2
NaOH	5 min	87 ± 4	23 ± 2
25 M in H_2O, rt	10 min	46 ± 5	59 ± 3
	30 min	43 ± 1	62 ± 0
	60 min	39 ± 0	66 ± 0
	120 min	37 ± 1	67 ± 1
	1200 min	42 ± 3	63 ± 2
H_2SO_4	5 s	104 ± 2	8 ± 2
18 M in H_2O, rt	10 s	88 ± 1*	22 ± 0
	20 s	81 ± 2*	29 ± 1

* with damaged threads

[a] % decrease in $\Theta = -(\Theta_{\text{after treatment}} - \Theta_{\text{before treatment}})*100/\Theta_{\text{before treatment}}$

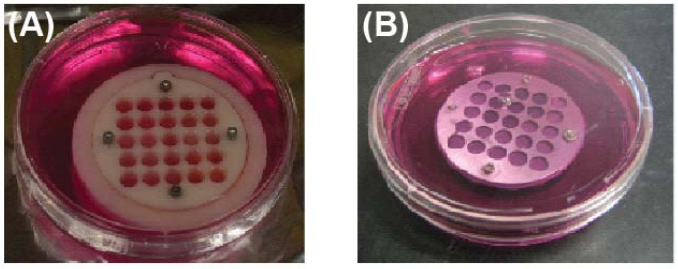

Figure S-3. Images showing the stacks of multi-zone mesh sheets using (A) acrylonitrile butadiene styrene (ABS)-based holders and (B) stainless steel holders.

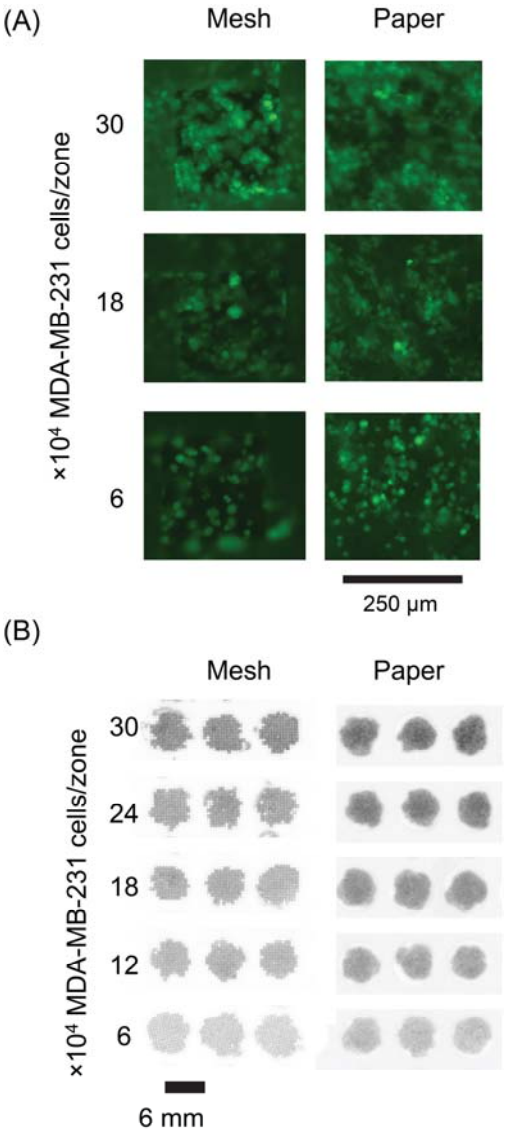
(A)
Mesh
Paper
30
18
6
×10⁴ MDA-MB-231 cells/zone
250 µm
(B)
Mesh
Paper
30
24
18
12
6
×10⁴ MDA-MB-231 cells/zone
6 mm
(C)
(ave. grayscale intensity-backgr.)×10⁴
30
25
20
15
10
5
0
mesh
y = 530x + 9500
R² = 0.999
paper
y = 610x + 11000
R² = 0.9889
0
5
10
15
20
25
30
×10⁴ MDA-MB-231 cells/zone

Figure S-4. Differences in densities of cells seeded onto polymer-based mesh supports using optical microscopy and fluorescence gel scanner. (A) Micrographs of cells stained with calcein cultured in CiGiM and CiGiP. The images shown here are representative magnified regions of a single zone to allow the morphology and density of the cells to be discerned clearly. (B) Scanned images from a fluorescence gel scanner of CiGiM and CiGiP showing zones containing the cells with varying cell densities. Only three out of the nine zones were shown for each concentration. (C) Plot showing the dependence of the grayscale intensity of the fluorescence signal of calcein with cell density. Each datum is an average of data measured from nine identical zones (n=9), containing the same concentrations of cells per zone.

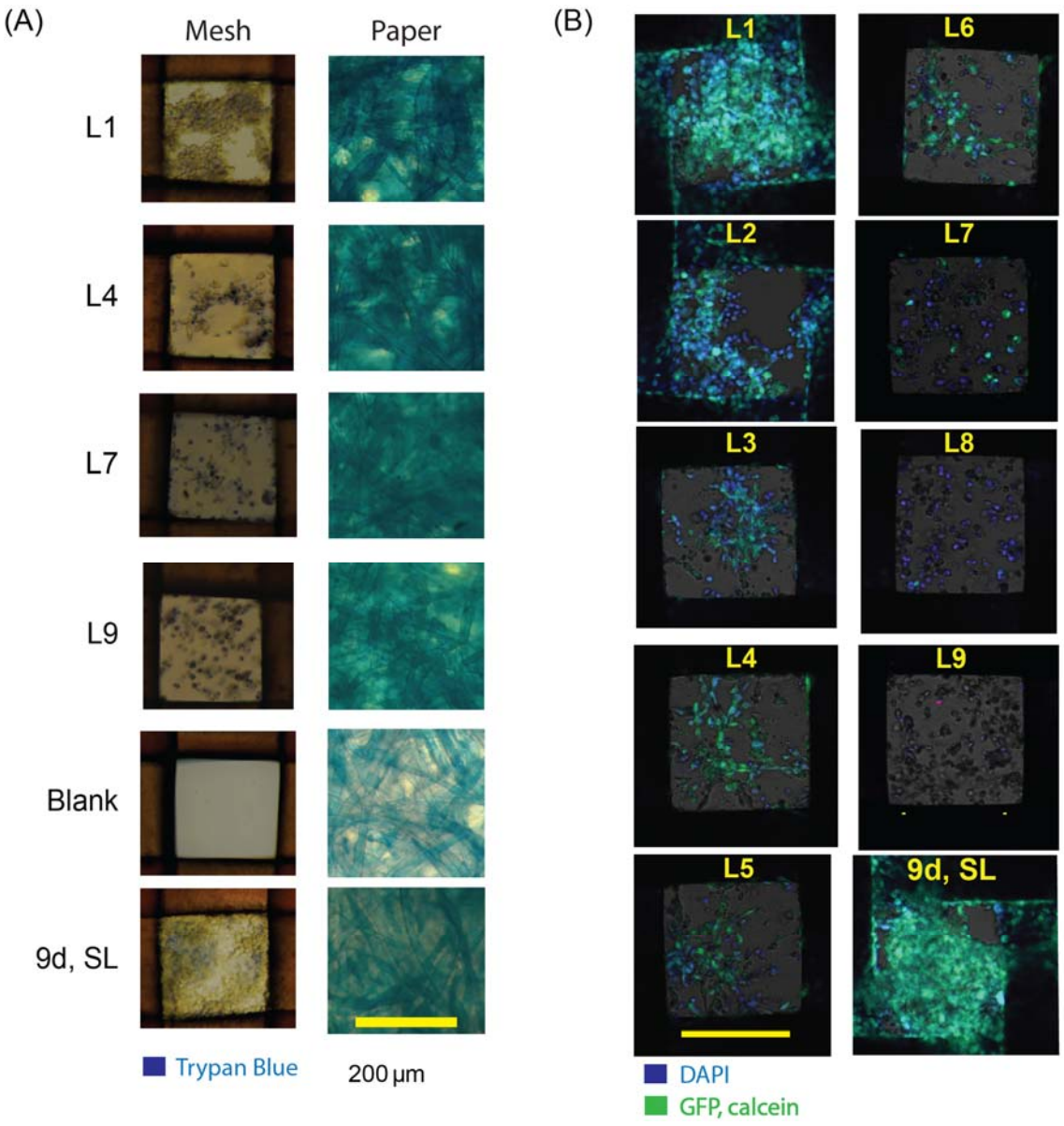
(A)
Mesh
Paper
L1
L4
L7
L9
Blank
9d, SL
Trypan Blue
200 μm
(B)
L1
L6
L2
L7
L3
L8
L4
L9
L5
9d, SL
DAPI
GFP, calcein

Figure S-5. Bright-field and confocal fluorescence micrographs of de-stacked layers of mutli-layered cultures. (A) Bright-field images of selected de-stacked layers (L1, L4, L7, L9) of CiGiM and CiGiP. The layers were incubated in Trypan Blue to stain dead cells with compromised membranes. For comparison, single layers of both mesh and paper which contained no cells and those seeded and cultured for 9 days without stacking are also shown. (B) Superimposed false-colored multichannel confocal fluorescence images (gray channel: bright field, green channel: calcein, blue channel: DAPI) showing a representative region of a zone from L1 to L9. For comparison, a layer that was cultured for 9 days without stacking is also shown. After staining with calcein, the layers were also fixed with paraformaldehyde and stained with DAPI prior to imaging with the confocal microscope.

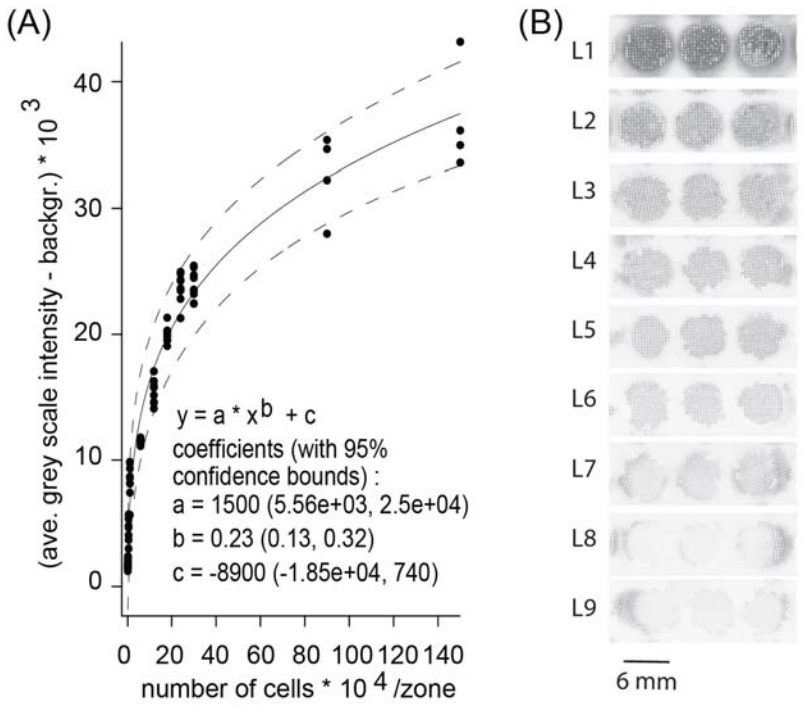

Figure S-6. Quantification of live cells based on calcein staining. (A) Calibration curve was generated by spotting known concentrations of MDA-MB-231-GFP on the zones of multi-zone mesh sheets. After staining the viable cells with calcein, we scanned and measured the intensities of the zones. The plotted values were calculated from the average intensities of the zones (n=9) minus the average intensity of the background. (B) Scanned images of representative calcein-stained zones of CiGiM from L1 to L9 after 9 days of culture and de-stacking. Figure S-8 shows images of all the zones from each layer.

Table S-2 Number of viable cells in de-stacked layers of multi-zone mesh after 9 days of culture

Layer (Lx)	mean $\times 10^4$ cells/mL	standard deviation $\times 10^4$ cells/mL	% decrease vs L1[a]	% cell death[b,c]
L1	73 ± 20	19.7	N/A	N/A
L2	10 ± 3	2.6	86	17
L3	5.8 ± 0.7	0.7	92	52
L4	3.8 ± 0.7	0.7	95	69
L5	3.2 ± 0.9	0.9	96	73
L6	1.4 ± 0.2	0.2	98	88
L7	1.6 ± 0.5	0.5	98	87
L8	0.5 ± 0.2	0.2	99	96
L9	0.5 ± 0.2	0.2	99	96

[a] % decrease vs L1 = (number of cells in L1 - number of cells in Lx)×100/number of cells in L1

[b] % cell death = (number of cells seeded- number of cells in Lx at the end of culture)×100/number of cells seeded

[c] number of cells seeded = 120,000 cells per zone

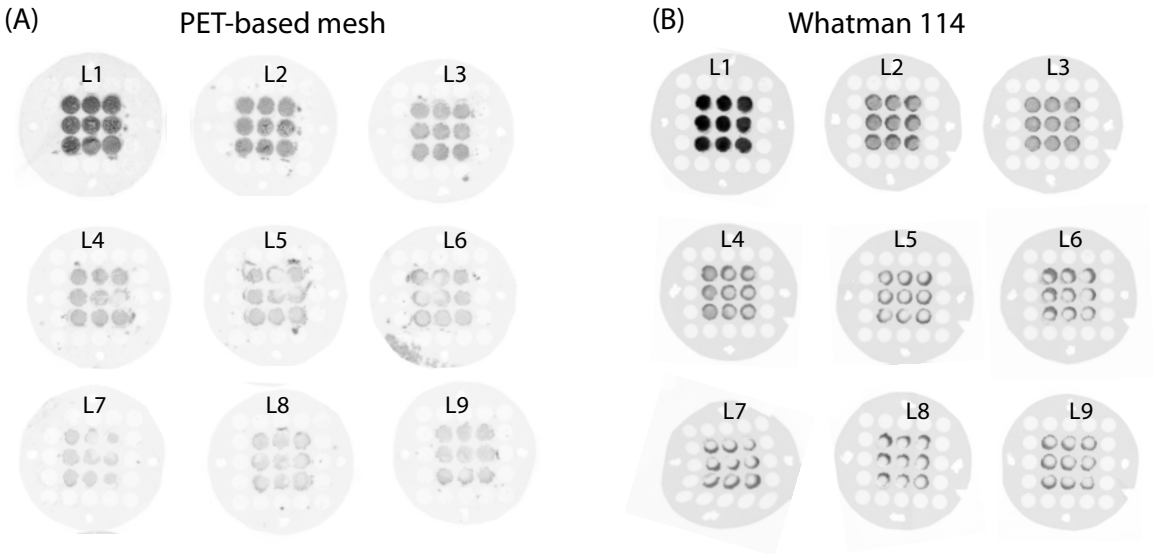

Figure S-7. Scanned images of the entire multi-layered stacks of constructs supported on (A) PET-based mesh with decal transferred Parafilm® barriers and (B) Whatman 114 with wax-printed barriers. Each set of the constructs consist of nine layers (L1 to L9) which comprise of nine middle zones that contain MDA-MB-231-GFP cells (initial cell density =120,000 cells/zone) and 16 surrounding zones that contain no cells. After culturing for 9 days, the constructs were de-stacked, stained with calcein, and imaged with a fluorescence gel scanner. The middle zones from each of these layers were cropped and included in Figure 3-C.

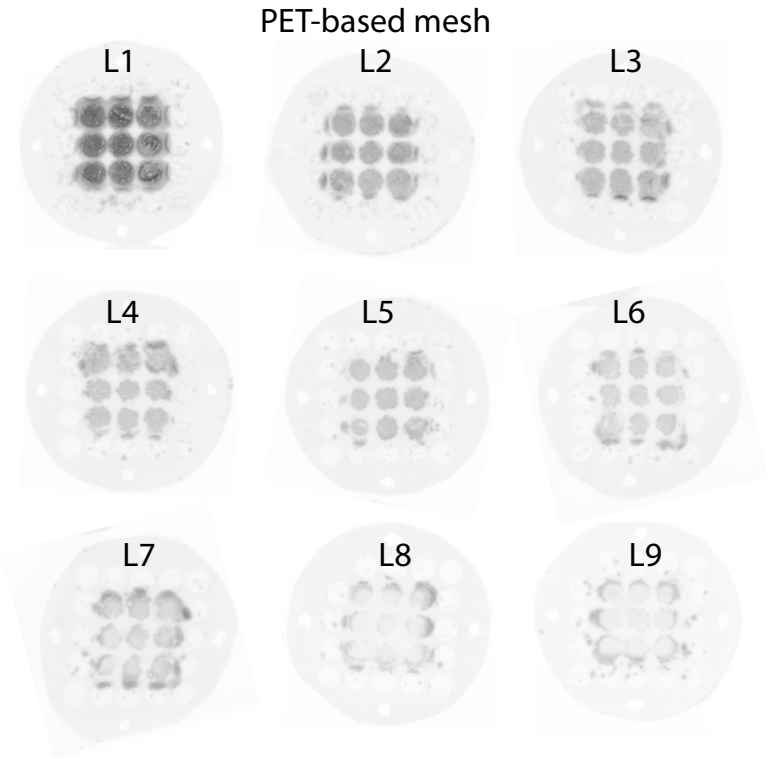

Figure S-8. Scanned images of the entire multi-layered stacks of MDA-MB-231-GFP constructs supported on mesh sheets patterned with decal-transferred Parafilm® barriers. Suspensions of MDA-MB-231-GFP cells in Matrigel (120,000 cells/zone) were seeded on the nine middle zones of each layer. The layers were incubated in warm media, stacked and cultured. After 9 days of culture, the layers were de-stacked, stained with calcein and imaged with a gel fluorescence scanner. The middle zones from each of these layers were cropped and included in Fig. S-5B. The intensities of each zone were measured and subtracted from the average intensity of the background. The number of viable cells from each layer (Fig. S-6C) were then calculated based on the calibration curve (Fig. S-6A) and the normalized intensity of the zones (n=9).

Simulation of the Oxygen Gradient in Stack

We estimated the gradient of oxygen in a CiGiM stack using the simulation software Comsol Multiphysics 4.3. We created a 3D finite element model (FEM) using the module for the transport of dilute species without convection. Therefore, mass transport in the system was diffusive and is described by Fick's law:

$$\frac{\partial c}{\partial t} + \nabla \cdot (-D\nabla c) = R \qquad \text{(Eq S-1)}$$

where c is the concentration of oxygen ($mol \cdot m^{-3}$), D is the diffusion coefficient ($m^2 \cdot s^{-1}$) of oxygen in Matrigel, R is the rate of reaction of oxygen ($mol \cdot m^{-3} \cdot s^{-1}$) in the system (which is equal to the rate of consumption by the cells), and ∇ is the standard del operator. Our model assumes a uniform distribution of cells within a zone composed of purely of Matrigel and surrounded by an oxygen impermeable mesh Parafilm® decal. The effect of the fibers of the mesh on the transport of oxygen through the stack was accounted for by multiplying the diffusion coefficient of the Matrigel by the percentage of open area of the mesh (i.e., 47%).

The stack consisted of nine layers; each layer was represented by a cylinder (diameter of 6 mm and height/thickness of 180 μm). The boundaries were set to a 'No Flux' condition. The top surface of the first layer was set to a constant concentration of 0.2 mM to match the dissolved concentration of oxygen in the media at ambient conditions. The diffusion coefficient of oxygen in the Matrigel was set to $1.59 \cdot 10^{-5}$ $cm^2 \cdot s^{-1}$ [1] based on the literature [1].

Each layer was set to have a reaction term, *R,* assuming Michaelis-Menten kinetics; the rate of consumption of oxygen by the cells is dependent on the concentration

of ambient oxygen [2, 3]. The equation that we used is shown as Equation 2, where, c signifies the concentration of oxygen in the stack.

$$R = \frac{-1.65 \cdot 10^{-4} \cdot c}{c + 1 \cdot 10^{-3}} \cdot \mathrm{flc1hs}(c - 1 \cdot 10^{-4}, 5 \cdot 10^{-5}) \quad \text{(Eq S-2)}$$

We set a maximum reaction rate of $-1.65 \cdot 10^{-4}$ ($mol \cdot s^{-1} \cdot m^{-3}$) for 120,000 cells per layer based on the experimentally measured consumption rate of MDA-MB-231 cells [4]; Michaelis-Menten constant ($k_{m,\,O2}$) of $1 \cdot 10^{-3}$ $mol \cdot m^{-3}$ was used based on other literature [5]. We also implement a step-down function, flc1hs(x, scale) to avoid creating negative concentrations of oxygen.

Figure S-9 shows the results of the concentration gradient of oxygen within a stack after reaching a steady state conditions. Figure S-10 shows a plot of the concentration of oxygen (normalized to the concentration of oxygen at the top surface of the stack) as a function of depth within the stack. Our simulations show that the concentration of oxygen in the stack drops from 0.2 mM (at the top of the stack) to < 0.001 mM (at a depth of ~1.39 mm from the top of the stack). We expect the real situation in a CiGiM stack to be more complicated since cells can migrate and die within the different layers. The cells can also change their metabolism based on the availability of growth factors or other nutrients.

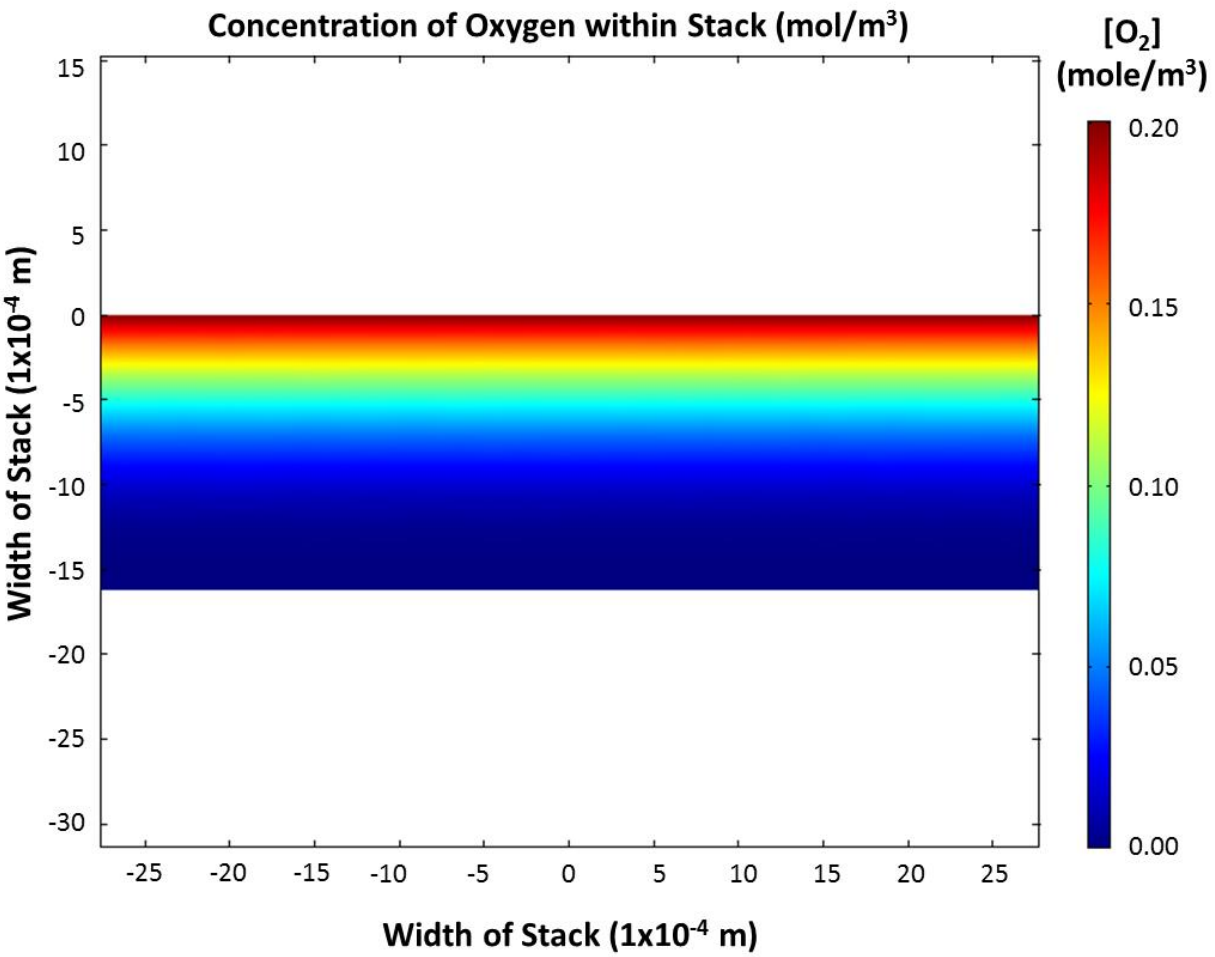

Figure S-9. Heat map depicting the concentration of oxygen for a stack of 9 layers at steady state in standard culture conditions. The colored rectangle represents a stack of zones with a diameter of 6 mm and a thickness of 180 μm. Each layer contains 120,000 MDA-MB-231 cells.

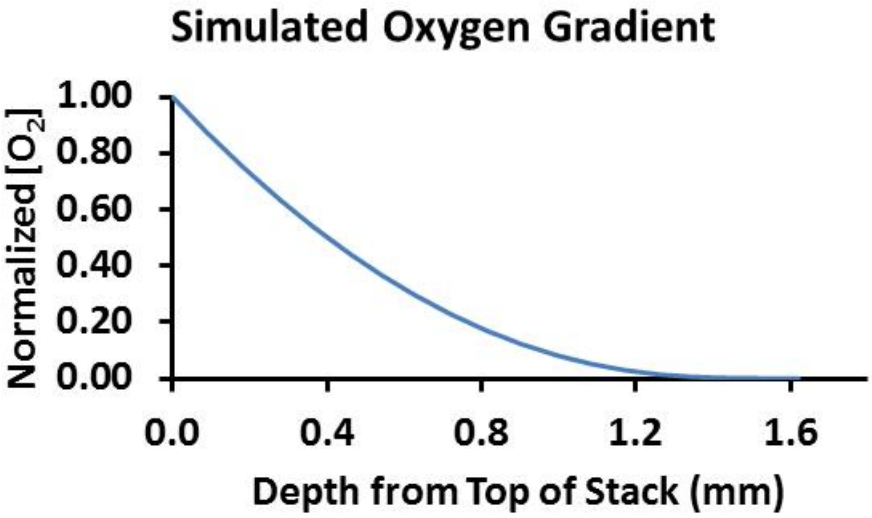

Figure S-10. Plot summarizing the concentration of oxygen calculated from FEM.

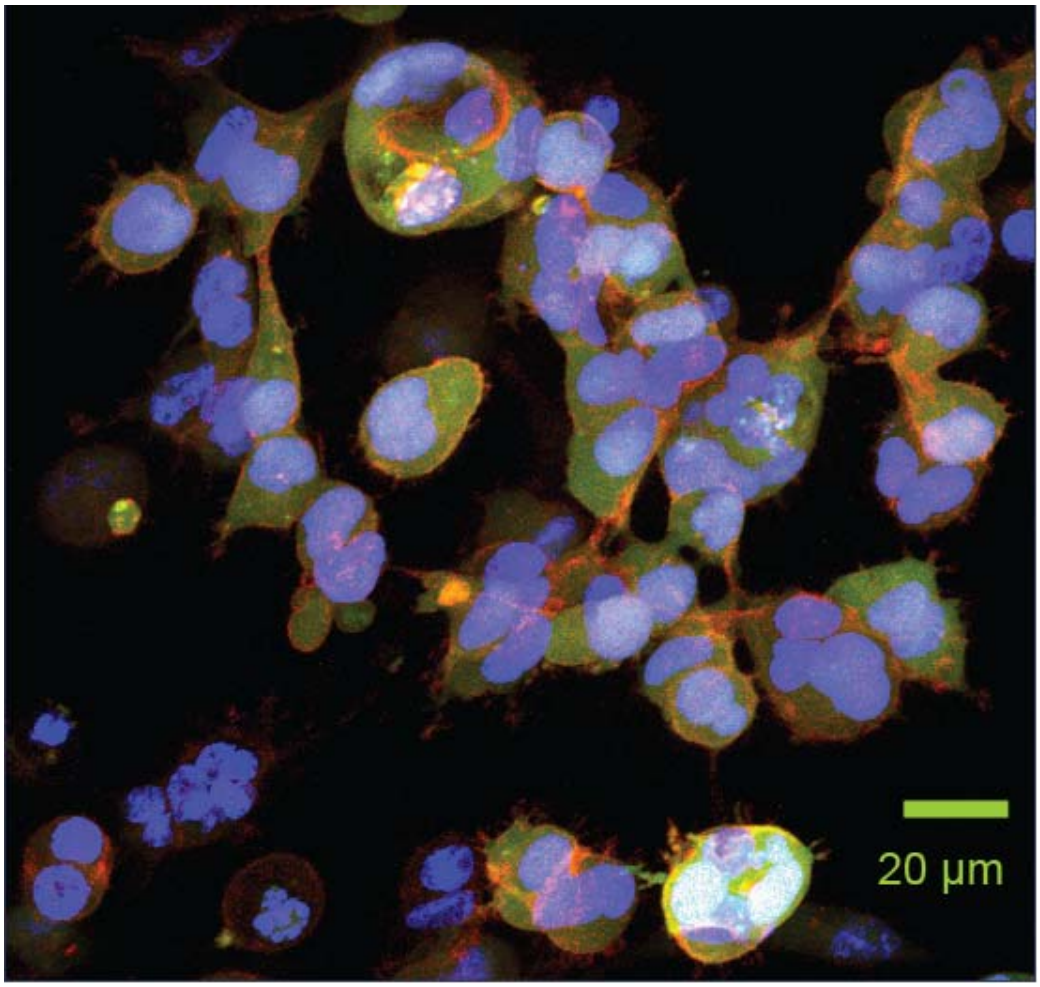

Figure S-11. Maximum intensity projection collected from a series of confocal fluorescence images of MDA-MB-231-GFP cells within the thickness (180 µm) of a PET mesh sheet (green channel: GFP, red channel: Alexa 633-phalloidin, blue channel: DAPI). Suspension of MDA-MB-231-GFP cells in Matrigel (30,000 MDA-MB-231-GFP cells/zone) were seeded into the zones of the mesh sheet and cultured for 2 days. At the end of the culture, the layers were fixed with paraformaldehyde (1 hour, room temperature), permeabilized with PBS containing 0.1% Triton X-100 (30 mins , 4°C), and blocked with PBS containing 2% BSA and 0.1% Triton X-100 (30 mins , 4°C). The layers were incubated in 1:500 dilution of phalloidin conjugated with Alexa 633 (2 hours at 4°C), washed twice with PBS, and stained with DAPI.

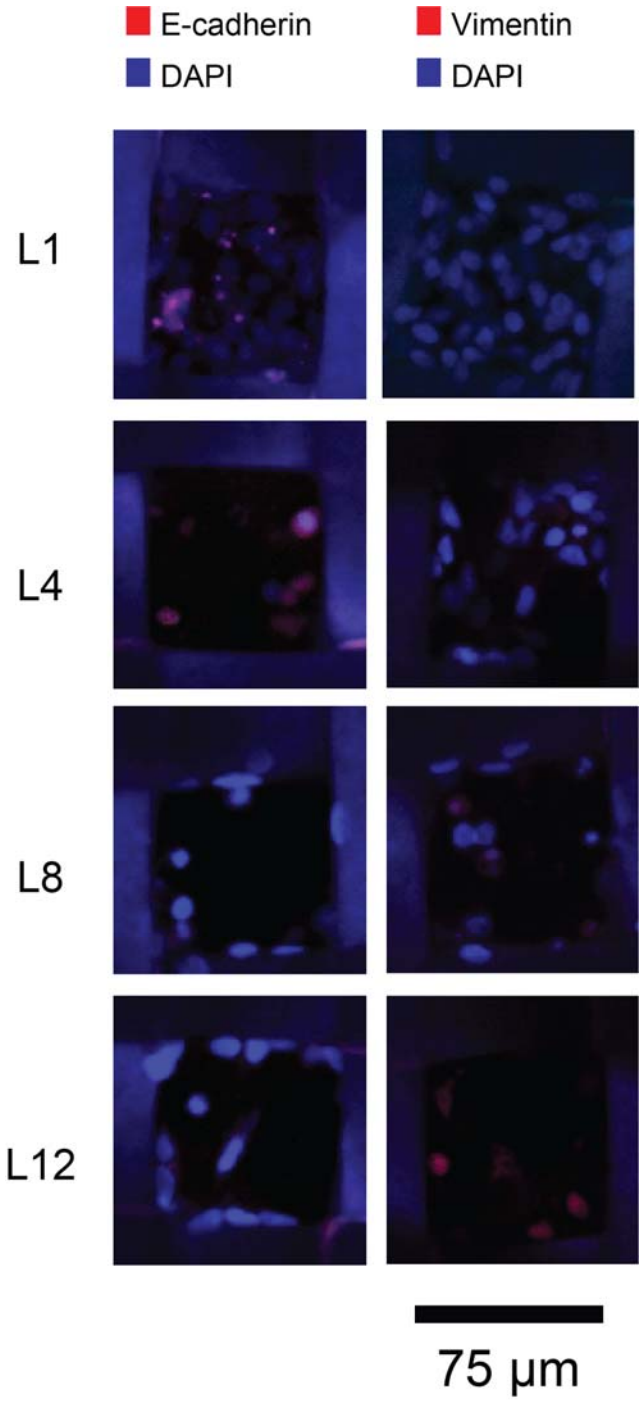

Figure S-12. Confocal fluorescence images of de-stacked multi-layered cultures of A549 non-small lung cancer cells. Two identical stacks were prepared to label A549 cells—one stack was labeled with anti-Ecadherin—a marker for epithelial cells, and another stack

was labeled with anti-Vimentin—a marker for mesenchymal cells [6]. Each set comprised of 12 layers that contain A549 cells (initial seeding density = 100,000 cells/zone). After culturing for 12 days, the constructs were de-stacked, fixed with paraformaldehyde (1 hour, room temperature), permeabilized with PBS containing 0.1% Triton X-100 (30 min, 4°C), and blocked with PBS containing 2% BSA and 0.1% Triton X-100 (30 min, 4°C). The layers were incubated in 1:100 dilutions of primary antibodies (anti-E-cadherin or anti-Vimentin, overnight at 4°C), and washed twice with PBS containing 2% BSA and 0.1% Triton X-100. We used 1:100 dilution of secondary antibody conjugated to Alexa Fluor 647 to stain epithelial (stained with anti-E-cadherin) and mesenchymal (stained with anti-Vimentin) cells in the samples. We mounted the layers using Vectashield+DAPI before imaging with the confocal microscope. The mesh sheets used in this experiment have a thickness of ~150 μm, and have openings with a diameter of ~75 μm.

References

1. Kim B, Han G, Toley BJ, Kim CK, Rotello VM, Forbes NS. Tuning payload delivery in tumour cylindroids using gold nanoparticles. Nat Nanotechnol. 2010 Jun;5(6):465-72.

2. Avgoustiniatos ES, Colton CK. Effect of external oxygen mass transfer resistances on viability of immunoisolated tissue. In: Prokop A, Hunkeler D, Cherrington AD, editors. Bioartificial Organs: Science, Medicine, and Technology1997. p. 145-67.

3. Wilson DF, Rumsey WL, Green TJ, Vanderkooi JM. The oxygen dependence of mitochondrial oxidative-phosphorylation measured by a new optical method for measuring concentration. J Biol Chem. 1988 Feb;263(6):2712-8.

4. Hahm ER, Moura MB, Kelley EE, Van Houten B, Shiva S, Singh SV. Withaferin A-Induced Apoptosis in Human Breast Cancer Cells Is Mediated by Reactive Oxygen Species. PloS One. 2011 Aug;6(8).

5. Buchwald P. FEM-based oxygen consumption and cell viability models for avascular pancreatic islets. Theoretical Biology and Medical Modelling. 2009 Apr;6.

6. Scanlon CS, Van TEA, Inglehart RC, D'Silva NJ. Biomarkers of epithelial-mesenchymal transition in squamous cell carcinoma. J Dent Res. 2013;92:114-21.